Colloquium: Electronic transport in single-crystal organic transistors

M. E. Gershenson and V. Podzorov

Department of Physics and Astronomy, Rutgers University, Piscataway, New Jersey 08854, USA

A. F. Morpurgo

Kavli Institute of Nanoscience, Faculty of Applied Sciences, Delft University of Technology, Lorentzweg 1, 2628 CJ Delft, The Netherlands

(Published 29 September 2006)

Small-molecule organic semiconductors, together with polymers, form the basis for the emerging field of organic electronics. Despite the rapid technological progress in this area, our understanding of fundamental electronic properties of these materials remains limited. Recently developed organic field-effect transistors (OFETs) based on single crystals of small-molecule organic materials are characterized by an unprecedented quality and reproducibility. These devices provide a unique tool to study the fundamentals of polaronic transport on organic surfaces and to explore the limits of OFET performance. This Colloquium focuses on the intrinsic, not limited by static disorder, charge transport in single-crystal OFETs and on the nature of defects on surfaces of organic crystals. In the conclusion, an outline of the outstanding problems that are now becoming within experimental reach owing to the development of single-crystal OFETs is presented.

DOI: 10.1103/RevModPhys.78.973 PACS number(s): 78.40.Me, 71.38.Ht, 71.20.Rv

CONTENTS

I. INTRODUCTION: FIELD EFFECT IN SMALL-MOLECULE ORGANIC SEMICONDUCTORS

Organic semiconductors represent a large class of solids consisting of organic oligomers or polymers. In this Colloquium, we focus on crystals of small organic molecules (mostly polyacenes containing typically two to ten benzene rings) held together in a solid by van der Waals forces. These small-molecule organic semiconductors, together with polymers, represent the material basis for the rapidly developing field of organic electronics (Shaw and Seidler, 2001; Agranovich and Bassani, 2003; Forrest, 2004; Hoppe and Sariciftci, 2004; Katz, 2004; Neuman *et al.*, 2004). It is believed that organic electronics will be able to successfully compete with inorganic electronics for applications that require mechanical flexibility, large area coverage, and inexpensive mass production (Sheats, 2004). Examples of organic electronic devices include "smart" cards, "electronic" paper, all-organic active-matrix LED displays, and organic solar cells (Forrest, 2004).

Because of the weak van der Waals bonding, many electronic properties of organic materials (e.g., the energy gap between the highest occupied and lowest unoccupied molecular orbitals, HOMO and LUMO, respectively) are determined by the structure of an isolated molecule (Kao and Hwang, 1981; Silinsh and Čápek, 1994; Pope and Swenberg, 1999). Weak intermolecular overlap of electronic orbitals leads to the narrow electronic bands (a typical bandwidth $W \sim 0.1$ eV is two orders of magnitude smaller than that in silicon) and a low mobility of carriers ($\mu \sim 1$–10 cm^2/V s at room temperature). Anisotropy of the transfer integrals between adjacent molecules reflects the low symmetry of the molecular packing in organic molecular crystals (OMCs). It is believed that the most adequate description of charge transport in these semiconductors is based on the concept of small polarons (see, e.g., Holstein, 1959; Emin, 1982; Silinsh and Čápek, 1994; Pope and Swenberg, 1999), electronic states with a correlation between the

electronic and lattice degrees of freedom at a scale of the order of a lattice constant.

After several decades of intensive research, our basic understanding of charge transport in small-molecule organic semiconductors remains limited. The complexity of transport phenomena in these systems is due to the polaronic nature of charge carriers and the strong interaction of small polarons with defects (Silinsh and Cápek, 1994). An especially challenging task is to develop an adequate model of high-temperature polaronic transport. At room temperature, which is typically comparable to or even higher than the characteristic phonon energies, lattice vibrations might become sufficiently strong to destroy the translational symmetry of the lattice. In this regime, the fluctuation amplitude of the transfer integral becomes of the same order of magnitude as its average value (Troisi *et al.*, 2005), the band description breaks down, and a crossover from the band-like transport in delocalized states to the incoherent hopping between localized states is predicted with increasing temperature (Kenkre *et al.*, 1989; Wu and Conwell, 1997; Fratini and Ciuchi, 2003; Deng and Goddard, 2004; Hannewald and Bobbert, 2004, 2005; da Silva Filho *et al.*, 2005). The benchmark for the study of charge transport in organic semiconductors was established by the time-of-flight (TOF) experiments with ultrapure polyacene crystals, such as naphthalene and anthracene (Karl, 2001). These experiments have demonstrated that the intrinsic (not limited by static disorder) charge transport can be realized in the bulk of these crystals. This transport regime is characterized with a rapid growth of the carrier mobility with decreasing temperature and a pronounced anisotropy of the mobility which reflects anisotropy of the intermolecular transfer integrals (Hannewald and Bobbert, 2004, 2005). Numerous applications, however, are dependent on the charge transport on the *surface* of organic semiconductors. The most important example is the organic field-effect transistor (OFET), in which field-induced charges move along the interface between an organic semiconductor and a gate dielectric. In these devices conduction truly occurs at the surface, as the thickness of the conducting channel does not exceed a few molecular layers (Dodabalapur *et al.*, 1995; Dinelli *et al.*, 2004; Kiguchi *et al.*, 2005).

The transport of field-induced carriers on organic surfaces may differ from "bulk" transport in many respects. For instance, the density of carriers in field-effect experiments can exceed that in bulk TOF measurements by many orders of magnitude, approaching the regime when the intercharge distance becomes comparable with the size of small polarons (see, e.g., Panzer and Frisbie, 2005). Interactions between the polaronic carriers may become important in this regime. Also, the motion of charge carriers in the field-induced conduction channel may be affected by the polarization of the gate dielectric (Houili *et al.*, 2005). Molecular packing on the surface can also be different from that in the bulk.

Exploration of the polaronic transport on organic surfaces is crucial for a better understanding of fundamental processes that determine operation and ultimate performance of organic electronic devices. This is a very pressing issue. On the one hand, the first all-organic devices, e.g., the active matrix displays based on organic light-emitting diodes and organic transistors, are expected to be commercialized within a few years (Forrest, 2004). On the other hand, our knowledge of transport properties of organic semiconductors is much more limited than that of their inorganic counterparts. This paradoxical situation contrasts sharply with the situation in inorganic electronics in the mid-1960s, when the first Si metal-oxide semiconductor field-effect transistor (MOSFETs) were developed (Riordan and Hoddeson, 1997).

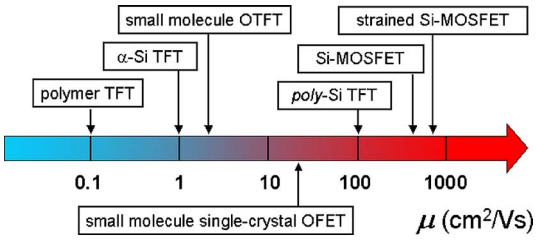

FIG. 1. (Color online) Charge-carrier mobility in field-effect transistors based on organic and inorganic semiconductors.

Fundamental research has been hampered by the lack of a proper tool for exploring the polaronic transport on surfaces of organic semiconductors. The most common organic electronic device whose operation relies on surface transport is the organic thin-film transistor (TFT). Over the past two decades a large effort in the development of TFTs has resulted in improvement in the characteristics of these devices (Horowitz, 2004), so that currently the best organic TFTs outperform the widely used amorphous silicon (α-Si:H) transistors. However, even in the best organic TFTs, charge transport is still dominated by the presence of structural defects and chemical impurities. As a result, it has been concluded that the TFTs "may not be appropriate vehicles for illuminating basic transport mechanisms in organic materials" (Nelson *et al.*, 1998).

Recently developed *single-crystal* organic transistors with significantly reduced disorder (Butko *et al.*, 2003; de Boer *et al.*, 2003; Podzorov, Pudalov, and Gershenson, 2003; Podzorov, Sysoev, *et al.*, 2003; Takeya *et al.*, 2003; Aleshin *et al.*, 2004; de Boer, Gershenson, *et al.*, 2004; Goldmann *et al.*, 2004; Sundar *et al.*, 2004) provide unique opportunities to explore fundamental processes that determine operation and reliability of organic electronic devices. For the first time, these single-crystal OFETs have enabled the observation of intrinsic (not limited by static disorder) transport of field-induced charges on organic surfaces (Menard *et al.*, 2004; Podzorov, Menard, Borissov, *et al.*, 2004; Podzorov, Menard, Rogers, and Gershenson, 2005). The carrier mobility in these devices is an order of magnitude greater than that in organic TFTs (Fig. 1). Equally important, the single-crystal OFETs are characterized by an unprecedented level of reproducibility: devices fabricated in different

laboratories exhibit very similar characteristics. This reproducibility, which is crucial for investigations on electronic properties of organic semiconductors, has never been achieved with thin-film devices, whose electrical characteristics are dependent on the details of fabrication processes.

In this Colloquium, we present a brief overview of the experimental results obtained with single-crystal OFETs over the last four years. Because we focus on the physics of electronic processes in these devices, many device-oriented issues will not be discussed here; we refer the reader to a recent review by de Boer, Gershenson, *et al.* (2004) for details on device fabrication and characterization. In Sec. II, we briefly describe the crystal growth and OFET fabrication techniques that preserve the high-quality, pristine surface of as-grown crystals. Section III focuses on the observation of intrinsic polaronic transport on the surface of organic crystals. Electronic defects at organic surfaces and mechanisms of their formation are discussed in Sec. IV. Section V outlines several basic issues that are now starting to be within experimental reach due to the development of single-crystal OFETs and for which theoretical work remains to be done.

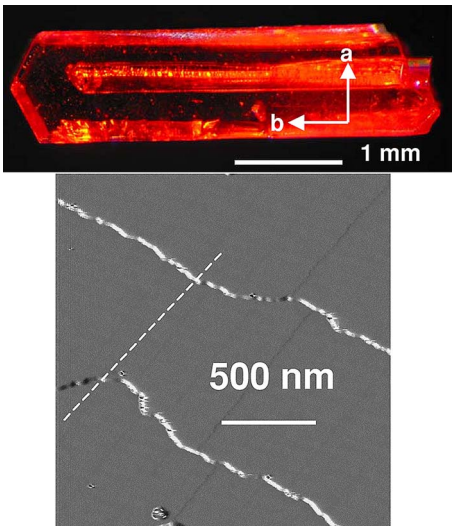

FIG. 2. (Color online) Vapor-grown rubrene single crystals. Top: Typical dimensions. Bottom: Atomic-force-microscopy image of the rubrene surface showing monomolecular growth steps oriented mostly along the ***b*** axis. The height of two consecutive steps is equal to the lattice parameter along the ***c*** axis (the unit cell includes two monomolecular layers) (Menard *et al.*, 2004).

II. FABRICATION OF SINGLE-CRYSTAL ORGANIC FETs

The starting point in the fabrication of single-crystal OFETs is the growth of ultrapure organic crystals. To ensure high purity, organic single crystals are grown by physical vapor transport (PVT) in a stream of ultrahigh purity argon, helium, or hydrogen gas (Laudise *et al.*, 1998). Typically, several purification cycles are required to achieve sufficiently low concentration of impurities. X-ray-diffraction studies show that most of the PVT-grown crystals are of excellent structural quality; they are characterized by a very small mosaic spread, typically, less than 0.05° (Zeis *et al.*, 2005); in rubrene this value has been found to be even smaller, ~0.015° (Chapman *et al.*, 2006).

Figure 2 shows an example of a vapor-grown small-molecule crystal: this is rubrene, which has so far demonstrated the highest mobility in single-crystal OFETs. Rubrene crystallizes in an orthorhombic structure with four molecules per unit cell and the lattice parameters $\boldsymbol{a}=14.44$ Å, $\boldsymbol{b}=7.18$ Å, and $\boldsymbol{c}=26.97$ Å (Henn *et al.*, 1971); crystallographic data for several common polyacenes have been reported by Campbell *et al.* (1962). The crystals are usually elongated along the ***b*** axis; the largest flat facet of the crystal corresponds to the $(\boldsymbol{a},\boldsymbol{b})$ plane. The density of surface defects in these crystals, which have a very high level of structural perfection in the bulk, is low; the most common type of surface defects are the monomolecular growth steps separated by a relatively large distance, ~1 μm (Menard *et al.*, 2004).

Fabrication of field-effect structures on the surface of organic crystals is a challenge, because conventional thin-film processes (such as sputtering, photolithography, etc.) introduce a large density of defects on the fragile organic surfaces. For this reason, the first high-quality single-crystal OFETs have been realized only recently, after the development of two innovative fabrication techniques (see the review by de Boer, Gershenson, *et al.* 2004).

The first technique is based on the use of an unconventional gate dielectric: thin polymeric film of parylene, which can be deposited from a vapor phase on the surface of an organic crystal at room temperature and forms a parylene/OMC interface with a low density of electronic defects. The conformal parylene coating on the crystal surface has the advantage of minimizing the probability of electrical shorts between the gate and electrodes, which is important in devices with colloidal graphite contacts. Single-crystal OFETs with parylene dielectric are very stable: for example, the characteristics of rubrene/parylene transistors remain unchanged after storing in air and in the dark for more than 2 years. These devices are free standing; among the advantages of this design are the reduction of substrate-related strain and the possibility to perform optical studies by illuminating the conduction channel through a (semi-) transparent gate electrode (Podzorov and Gershenson, 2005).

In the second technique, the transistor circuitry is prefabricated by conventional microfabrication methods on a substrate, and an organic single crystal is subsequently laminated to such a "stamp." This technique eliminates the need for deposition of metal contacts and dielectrics directly onto organic crystals. Hard inorganic (Si) and flexible elastomeric [polydimethylsiloxane (PDMS)] stamps have been used for this purpose (see, e.g., de Boer, Gershenson, *et al.*, 2004). Elastomeric stamps compare favorably with Si stamps in two respects. First, because of their mechanical flexibility, PDMS stamps en-

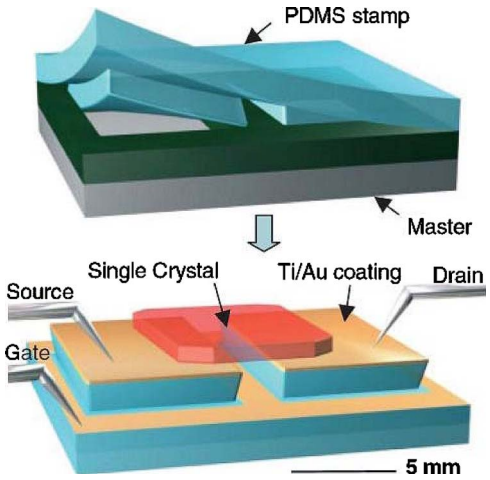

FIG. 3. (Color online) Fabrication of the air-gap OFET (Menard *et al.*, 2004). Top: Casting and curing a polymer (PDMS) against a pattern of photoresist on a silicon wafer defines an elastomeric stamp. Bottom: Coating this stamp with a collimated flux of metal produces electrically isolated source and drain electrodes (raised regions) together with a self-aligned gate electrode (recessed region). Lamination of an organic crystal against the stamp completes the fabrication process. The recessed gate electrode is separated from the conductive channel by a micron-size gap.

able establishing a good contact with crystals of various shapes and thickness even if the crystal surface is not perfectly flat. Second, for robust crystals such as rubrene, PDMS stamps provide a unique opportunity to reestablish the contact many times without noticeable degradation of the crystal surface. However, the density of field-induced charges achievable is typically greater in Si-based stamps, especially if these stamps utilize the high-ε gate insulators (Stassen *et al.*, 2004; de Boer, Iosad, *et al.*, 2005); this is important for exploring the regime of high carrier densities in which novel electronic phases might emerge.

Even though the lamination of crystals on prefabricated substrates enables a "low-impact" probing of charge transport on organic surfaces, this impact may still be too strong for most chemically reactive organic materials [e.g., a strong electron acceptor tetracyanoquinodimethane (TCNQ)]. To minimize these effects and to preserve the pristine surface of organic crystals, modification of the PDMS stamping technique has been recently introduced (Menard *et al.*, 2004), which allows avoiding these complications simply by eliminating the direct contact between the crystal and gate dielectric. The idea of this stamping technique is illustrated in Fig. 3. In these devices, the conventional solid gate dielectric is replaced by a micron-size gap between the gate electrode and surface of organic semiconductor. A thin layer of a gas (e.g., air) or vacuum between the bottom surface of the crystal and the recessed gate electrode plays the role of the gate dielectric. This approach does not only eliminate surface defects introduced in the process of lamination, but also enables studying the effect of different gases and other environmental agents on the conduction channel of single-crystal OFETs (Podzorov, Menard, *et al.*, 2005).

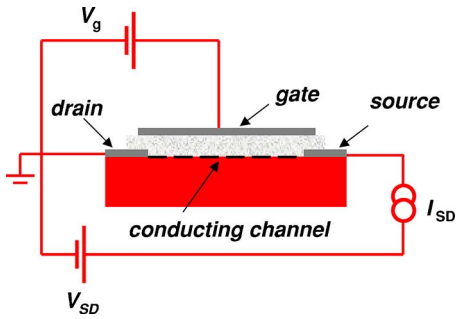

FIG. 4. (Color online) The field-effect transistor with the measuring circuit: V_G is the gate voltage, V_{SD} and I_{SD} are the source-drain voltage and current, respectively.

III. CHARGE TRANSPORT ON THE SURFACE OF ORGANIC SINGLE CRYSTALS

In this section, after a "primer" on the FET operation, we outline the main signatures of intrinsic polaronic transport observed in experiments with single-crystal OFETs and compare them to results of TOF and space-charge limited current (SCLC) experiments that probe charge transport in the bulk.

A. Basic FET operation

Contemporary OFETs are based on undoped organic semiconductors, and mobile charges in these devices must be injected from metallic contacts. These devices can potentially operate in both *electron*- and *hole*-accumulation modes, depending on the polarity of the gate voltage (the so-called *ambipolar* operation). Often, however, the injection barrier at the contact or the field-effect threshold for either *n*- or *p*-type conductivity is so large that an FET operates in a unipolar mode. For this reason, we mainly discuss the *p*-type conductivity, which is more commonly observed in OFETs.

A generic field-effect transistor is schematically shown in Fig. 4. With an increase of the gate voltage $|V_G|$ towards the threshold value $|V_G^{\rm th}|$, the injection of holes from metallic contacts depopulates localized electronic states (the deep traps, see Fig. 5) whose energies are separated from the edge of the HOMO band by more than a few k_BT. Note that this simplified model assumes the existence of the HOMO band; this assumption may be violated at high temperatures (Hannewald and Bobbert, 2004; Troisi and Orlandi, 2006). As a result, the Fermi level at the organic surface $E_{\rm F}$, initially positioned within the HOMO-LUMO gap, approaches the edge of the HOMO band $E_{\rm HOMO}$, which corresponds to the zero energy in Fig. 5. As soon as $E_{\rm F}-E_{\rm HOMO}$ becomes smaller than $\sim k_BT$, the OFET conductance increases by several orders of magnitude because holes are generated in the HOMO band due to the thermal excitation of carriers from the band into empty localized states. As a

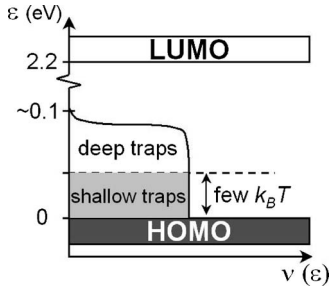

FIG. 5. Schematic diagram of the energy distribution of localized electronic states in the energy gap between HOMO and LUMO bands in rubrene single-crystal OFETs (Podzorov, Menard, *et al.*, 2004).

result, a ***p***-type conduction channel is formed at the interface between the semiconductor and gate dielectric. Overall device operation depends, to a large extent, on the energetics of semiconductor bands and metal contacts, therefore studies on the electronic structure of molecular interfaces are important (Cahen *et al.*, 2005).

Figure 6 shows the transconductance characteristics (i.e., the dependence of the source-drain current I_{SD} on the gate voltage V_G, measured at a constant source-drain voltage V_{SD}) and $I_{SD}(V_{SD})$ characteristics typical for *p*-type rubrene single-crystal OFETs (Podzorov, Pudalov, and Gershenson, 2003; Podzorov, Sysoev, *et al.*, 2003; Menard *et al.*, 2004). The channel conductance per square, $\sigma \equiv (I_{SD}/V_{SD})L/W$, increases linearly with V_G at $|V_G| > |V_G^{th}|$ (here L and W are the length and width of

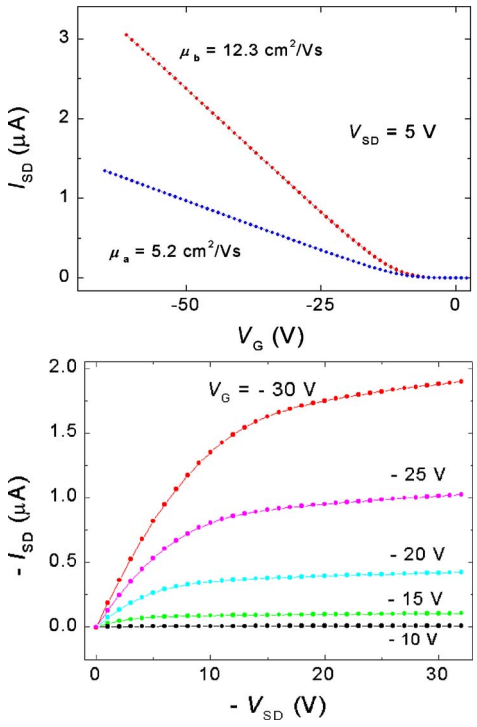

FIG. 6. (Color online) Characteristics of rubrene single-crystal OFETs: transconductance $I_{SD}(V_G)$ (upper panel) and $I_{SD}(V_{SD})$ (lower panel) [see, e.g., Menard *et al.* (2004) and Podzorov, Sysoev, *et al.* (2003)].

the conduction channel, respectively). This indicates that the carrier mobility (Sze, 1981)

$$\mu \equiv \frac{\sigma}{en} = \left(\frac{1}{C_i V_{SD}}\right)\left(\frac{dI_{SD}}{dV_G}\right)\frac{L}{W} \tag{1}$$

does not depend on the density of carriers field-induced above the threshold,

$$n = C_i(V_G - V_G^{th})/e. \tag{2}$$

Here C_i is the capacitance per unit area between the gate electrode and conduction channel.

A density-independent μ has been observed in devices based on single crystals of rubrene (Podzorov, Sysoev, *et al.*, 2003; Goldmann *et al.*, 2004; Sundar *et al.*, 2004), pentacene (Butko *et al.*, 2003; Takeya *et al.*, 2003), tetracene (de Boer *et al.*, 2003), and TCNQ (Menard *et al.*, 2004). This important characteristic of single-crystal OFETs contrasts sharply with a strongly V_G-dependent mobility observed in organic TFTs (Horowitz *et al.*, 2000) and amorphous silicon (α-Si:H) FETs (Shur *et al.*, 1989). In the latter case, the density of localized states within the gap is so high that the Fermi level remains in the gap even at high $|V_G|$ values. Observation of a V_G-independent mobility in single-crystal OFETs suggests that charge transport in these structures does not require thermal activation to the mobility edge. This is consistent with an increase of the mobility with cooling which is observed for high-quality single-crystal OFETs (see Sec. III.D) (for comparison, μ decreases exponentially with lowering temperature in organic and α-Si:H TFTs). The pronounced difference in the V_G and T dependences of the mobility in these two types of devices indicates that theoretical models developed for charge transport in α-Si:H or organic thin-film FETs (Shur *et al.*, 1989) are not applicable to single-crystal organic FETs.

For several important applications, including the implementation of CMOS technology in plastic electronics, it is important to achieve ambipolar operation in OFETs. However, most organic FETs operate in the *p*-type mode, and examples of the *n*-type operation with high mobility are rare (Chesterfield *et al.*, 2003; Menard *et al.*, 2004). This "asymmetry" between *n*- and *p*-type carriers is caused by a stronger trapping of *n*-type polarons (Karl, 2001) and a larger Schottky barrier for electron injection into organic semiconductors from most large-work-function metal contacts (Cahen *et al.*, 2005).

Figure 7 illustrates the *n*-type operation in a single-crystal TCNQ transistor. The surface of TCNQ, a semiconductor with a very high electron affinity, can be easily damaged: For example, direct contact of the crystal with PDMS stamps results in a very poor transistor performance with electron mobilities $\sim(2-3)\times10^{-3}$ cm^2/V s. "Air-gap" PDMS stamps (Menard *et al.*, 2004) help to solve the problem: the observed carrier mobility $\sim$1.6 cm^2/V s is significantly higher than in most *n*-channel organic TFTs. The mobility, however, is still limited by trapping; more work is required to approach the fundamental performance limit of *n*-type OFETs.

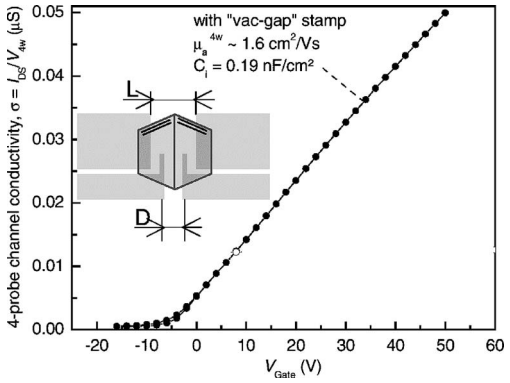

FIG. 7. Channel conductivity along the ***a*** axis of TCNQ single crystal measured in a vacuum-gap OFET (Menard *et al.*, 2004). The mobility of *n*-type carriers is 1.6 cm^2/V s.

Potentially, ambipolar transistors can be used for the development of electroluminescent optoelectronic devices: The *n*- and *p*-type carriers, being simultaneously injected in the conduction channel, can recombine and emit light [see, e.g., Nakamura *et al.* (2005), and references therein]. In practice, realization of ambipolar operation is a challenge because two difficult problems must be solved simultaneously: (i) the density of both *n*- and *p*-type traps should be minimized at organic/dielectric interfaces, and (ii) an effective injection of both *n*- and *p*-type carriers from contacts into the organic semiconductor must be realized. Among inorganic FETs, only devices based on carbon nanotubes (Misewich *et al.*, 2003) and single crystals of transition-metal dichalcogenides (Podzorov, Gershenson, *et al.*, 2004) demonstrated high-mobility ambipolar operation. The number of organic materials in which the ambipolar operation has been demonstrated is also limited (Chesterfield *et al.*, 2003; Meijer *et al.*, 2003; Chua *et al.*, 2005; Yasuda and Tsutsui, 2005). Organic single crystals, with their intrinsically low density of traps, offer a unique opportunity to realize ambipolar operation with a (relatively) high mobility of both carrier types.

Ambipolar operation has been recently observed in single-crystal OFETs based on metal phthalocyanine (MPc), namely, FePc and CuPc (de Boer, Stassen, *et al.*, 2005) (Fig. 8) and rubrene (Takahashi *et al.*, 2006). Because of a relatively small HOMO-LUMO gap in these materials, both electrons and holes can be injected into the organic semiconductor from the source and drain electrodes made of the same metal. Although the performance of the ambipolar single crystal devices is still dominated by extrinsic factors, the mobility observed for holes and electrons [respectively, 0.3 and 0.03 cm^2/V s for FePc (de Boer, Stassen, *et al.*, 2005), 1.8 and 0.01 cm^2/V s for rubrene (Takahashi *et al.*, 2006)] compare favorably with that in the ambipolar thin-film transistors. Note also that the low density of traps on the interface between a single crystal and gate dielectric facilitates observation of ambipolar operation. For comparison, the CuPc-based TFTs, which have been the subject of many past investigations (Bao *et al.*, 1996), demonstrate only *p*-type operation (presumably, because of a high density of *n*-type traps in these devices).

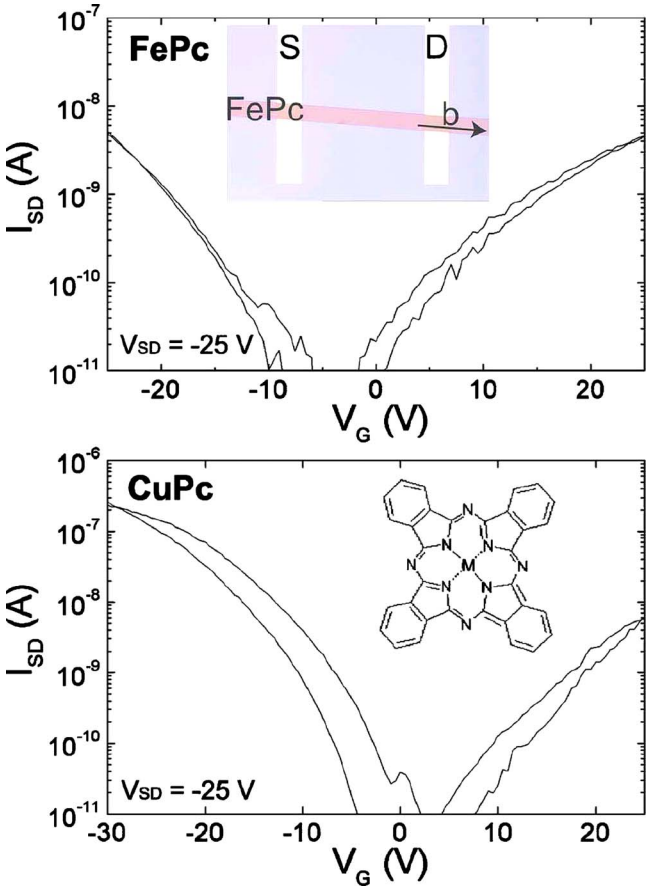

FIG. 8. (Color online) Transconductance characteristics of FePc and CuPc single-crystal FETs with gold electrodes (de Boer, Stassen, *et al.*, 2005). The hole mobilities reach ~0.3 cm^2/V s for both FePc and CuPc, the electron mobilities are 3×10^{-2} and 1×10^{-3} cm^2/V s, respectively.

In general, the performance of FET devices is characterized by many parameters including mobility, threshold voltage, the on/off ratio, and the subthreshold slope (Sze, 1981; de Boer, Gershenson, *et al.*, 2004). Here we focus on the first two parameters—the mobility μ and the threshold voltage V_G^{th}, because they are the most relevant to the physics of charge transport on the surface of organic semiconductors. Note that with respect to other parameters (e.g., subthreshold slope), single-crystal OFETs also compare favorably with organic and inorganic TFTs (see, e.g., Podzorov, Sysoev, *et al.*, 2003); these application-relevant issues are beyond the scope of this Colloquium.

B. Multiple trap-and-release model

Although the density of structural defects in the conduction channel of single-crystal OFETs is significantly lower than in organic TFTs, defects are still present. These defects create localized electronic states in the HOMO-LUMO gap that are schematically shown in Fig. 5 (the electronic defects will be discussed in Sec. IV).

The effect of these states on charge transport depends on their energy. If the energy of a localized state is separated from the mobility edge by more than a few k_BT, the state acts as a deep trap: The charge, once trapped in a deep trap, cannot be released by thermal excitations. For the pristine surface of rubrene single crystals at room temperature, for instance, the density of deep traps can be as low as 10^{10} cm^{-2} (Podzorov, Menard, *et al.*, 2004). On the contrary, trap states with energies within a few k_BT near the mobility edge (*shallow traps*) are characterized with a finite trapping time: After being trapped for a characteristic time τ_{tr}, a polaron can be thermally activated to the mobility edge.

At a phenomenological level, the effect of shallow traps on the channel conductivity can be described with the multiple trap-and-release (MTR) model (Bube, 1960; Horowitz, 2004). According to this model, which helps to illustrate the distinction between "intrinsic" and trap-dominated transport, not all the charges field induced above the threshold ($|V_G|>|V_G^{th}|$) contribute to current flow at any given moment of time. Some mobile charges can be momentarily trapped by shallow traps; the number of these charges depends on the energy and density of shallow traps as well as on temperature.

Within the MTR model, the effect of trapping can be described using two approaches. One can assume that all carriers field induced above the threshold voltage contribute to the current flow, but their effective mobility μ_{eff} is reduced in comparison with its intrinsic, trap-free value μ_0:

$$\mu_{eff} = \mu_0(T)\frac{\tau(T)}{\tau(T)+\tau_{tr}(T)}. \quad (3)$$

Here $\tau(T)$ is the average time that a polaron spends traveling between shallow traps. Alternatively, one can assume that only a fraction of the carriers field induced above the threshold voltage are moving at any given moment of time,

$$n_{eff} = n\frac{\tau(T)}{\tau(T)+\tau_{tr}(T)}, \quad (4)$$

but these charges are moving with the intrinsic mobility μ_0. These two approaches are equivalent for describing the channel conductivity $\sigma=en\mu$, which only depends on the product of n and μ. The distinction between these approaches becomes clear in Hall-effect measurements, in which the density and mobility of mobile charges can be determined independently (see Sec. III.D).

According to Eq. (3), the intrinsic regime of conduction occurs when $\tau \gg \tau_{tr}$: In this case, $\sigma(T)$ reflects the temperature dependence of intrinsic mobility $\mu_0(T)$. In the opposite limit $\tau \ll \tau_{tr}$, transport is dominated by trapping and release processes. It will be shown below that the intrinsic regime is characterized by a large anisotropy of the charge transport, an increase of the mobility with decreasing temperature, and a conventional nonactivated Hall effect.

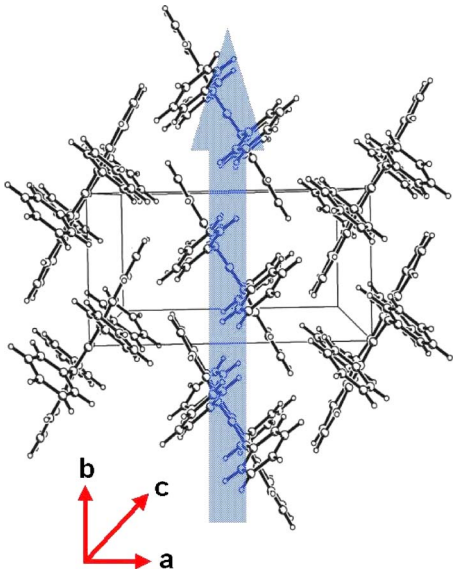

FIG. 9. (Color online) Packing of molecules in rubrene crystals (Sundar *et al.*, 2004). The crystal facets used for the FET fabrication correspond to the ***a*-*b*** crystallographic plane; the largest μ is observed for charge transport along the ***b*** axis.

C. Anisotropy of the mobility

Polyacenes typically form crystals with a herringbone packing of molecules (the molecular packing in rubrene crystals is shown in Fig. 9). Transfer integrals between adjacent molecules in these crystals vary significantly depending on the crystallographic direction (Brédas *et al.*, 2002; Cheng *et al.*, 2003; de Wijs *et al.*, 2003). This leads to a strong anisotropy of organic crystal transport properties, which has been well documented in TOF experiments (Karl, 2001). However, prior to the development of single-crystal OFETs, anisotropy had never been observed in the field-induced transport on the surface of organic semiconductors.

Several types of single-crystal OFETs based on rubrene demonstrate anisotropy of surface conductivity (Podzorov, Menard, *et al.*, 2004; Sundar *et al.*, 2004; Zeis *et al.*, 2006). In rubrene devices based on PDMS stamps, mobility along the crystallographic ***b*** axis exceeds mobility along the ***a*** axis by a factor of ~3 (Fig. 10) (Sundar *et al.*, 2004). A similar ratio μ_b/μ_a has been observed for rubrene transistors with the parylene gate dielectric (Zeis *et al.*, 2006). Clear correlation between the mobility and molecular packing has also been observed recently for a family of tetrathiafulvalene derivatives (Mas-Torrent *et al.*, 2004).

A small density of shallow traps in the single-crystal rubrene OFETs facilitated observation of the mobility anisotropy. However, even in these devices anisotropy of effective mobility μ_{eff} vanishes at lower temperatures (Fig. 11), where charge transport becomes dominated by traps. To explain the vanishing of mobility anisotropy within the MTR model, one should take into account that τ_x, the time of travel between shallow traps along a certain crystallographic direction ***x***, is inversely propor-

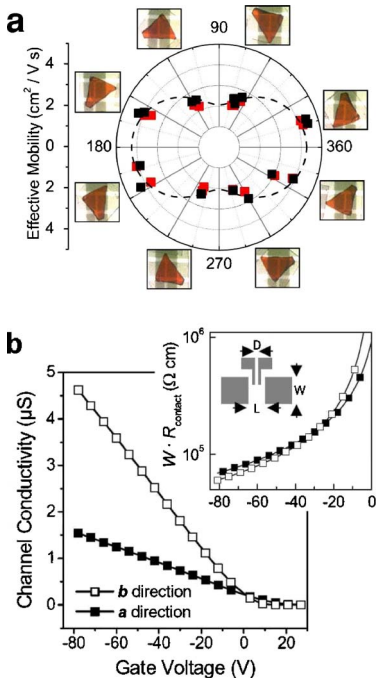

FIG. 10. (Color online) Anisotropy of charge transport along the ***a***-***b*** plane in rubrene crystals. (a) Polar plot of the mobility (the angle is measured between the ***b*** axis and direction of current flow). (b) Four-probe measurements of the channel conductivity and the contact resistance (inset) as a function of V_G along the ***b*** and ***a*** axes; μ values measured along the ***b*** and ***a*** axes are 15.4 and 4.4 $cm^2/V\,s$, respectively (Sundar *et al.*, 2004).

tional to the intrinsic mobility along this direction, μ_0^x. In the trap-dominated regime ($\tau \ll \tau_{tr}$), Eq. (3) is reduced to $\mu_{eff}=\mu_0^x \tau_x/\tau_{tr}$, and μ_{eff} does not depend on the crystallographic direction. The higher the shallow trap density, the narrower the temperature range where mobility anisotropy can be observed.

Qualitatively, the observed anisotropy of μ in rubrene can be explained on the basis of the molecular packing in these crystals (Fig. 9). Due to the co-facial orientation of molecules in stacks along the ***b*** axis, charge motion along the stacks is facilitated in comparison with that in

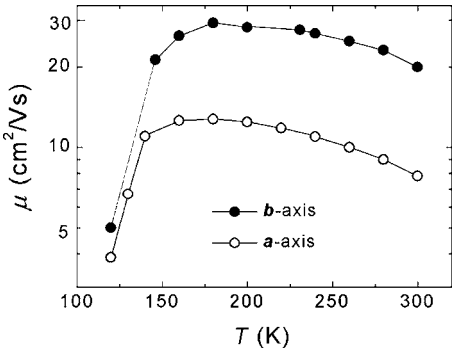

FIG. 11. Temperature dependences of the mobility in rubrene OFET extracted from four-probe measurements of the conductivity along the ***a*** and ***b*** axes (Podzorov, Menard, *et al.*, 2004).

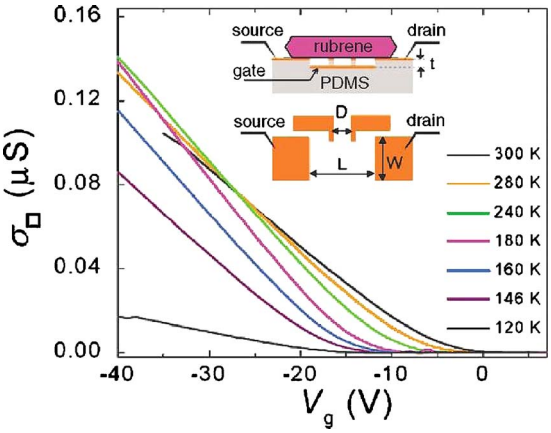

FIG. 12. (Color online) Sheet conductivity $\sigma_{\square}$ of a vacuum-gap rubrene single-crystal OFET, measured as a function of V_G at different T using the four-probe technique (Podzorov, Menard, *et al.*, 2004).

the perpendicular direction. Recent calculations of the band structure of rubrene based on the methods of quantum chemistry confirmed that the transfer integral values reach a maximum for the ***b*** axis (da Silva Filho *et al.*, 2005). For the quantitative description of the mobility anisotropy and its temperature dependence, *ab initio* calculations that take into account both intramolecular and intermolecular vibrations are needed; currently, such calculations are available only for bulk conduction in crystals of linear polyacenes (naphthalene, anthracene, and tetracene) (Hannewald and Bobbert, 2004, 2005).

D. Longitudinal and Hall conductivity in rubrene OFETs

The intrinsic and trap-dominated transport regimes in single-crystal OFETs can be identified by measuring the conductivity over a wide temperature range. The longitudinal conductivity of high-quality rubrene single-crystal OFETs, measured at different T as a function of V_G, is shown in Fig. 12. Assuming that all charges field induced above the threshold participate in the current flow, one can attribute the observed T variations of the slope $d\sigma/dV_G$ to the nonmonotonic temperature dependence of the effective mobility $\mu_{eff}=\sigma/en$ (see Fig. 11). The increase of μ_{eff} with cooling observed in the range $200<T<300$ K is a signature of the intrinsic regime; the rapid drop of μ_{eff} below 160 K indicates a crossover to the trap-dominated regime. Note that for the device whose conductivity is shown in Fig. 12, the density of shallow traps N_{tr}^{sh}, which can be estimated from the temperature dependence of the threshold voltage $V_G^{th}(T)$, is relatively low ($N_{tr}^{sh}\sim 10^{10}$ cm^{-2}). For devices with higher N_{tr}^{sh}, the crossover between intrinsic and trap-dominated regimes occurs at higher temperatures. As a result, devices with $N_{tr}^{sh}\geq 10^{11}$ cm^{-2} demonstrate an activated temperature dependence of μ_{eff} even at room temperature, and the effective mobility is smaller than μ_0 (Podzorov, Pudalov, and Gershenson, 2003).

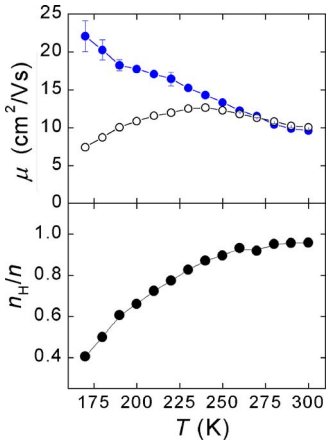

FIG. 13. (Color online) Hall mobility and carrier density extracted from the Hall measurements with rubrene single-crystal OFETs. Upper panel: Temperature dependences of the Hall mobility μ_H (solid circles) and the effective mobility μ_{eff} extracted from the longitudinal FET conductivity by calculating the density of mobile charges n using Eq. (2) (open circles). Lower panel: Temperature dependence of the ratio of the Hall carrier density n_H to the density n (Podzorov, Menard, Rogers, and Gershenson, 2005).

A better understanding of the intrinsic transport regime can be gained from measurements of the transverse (Hall) conductivity. An advantage of Hall measurements is that they allow independent measurements of n and μ. These measurements, however, are complicated by a very high sheet resistance of the conduction channel in OFETs, which often exceeds 10 M Ω/square. Only recently, Hall data became available for rubrene single-crystal (Podzorov, Menard, Rogers, and Gershenson, 2005; Takeya *et al.*, 2005).

The quantity n_H determined in Hall measurements is the density of charges that are moving at a given moment, i.e., n_H coincides with n_{eff} given by Eq. (4). The charges that are temporarily trapped in shallow traps do not contribute to the Hall voltage, because the Lorentz force, proportional to the carrier velocity, is equal to zero for these charges. Figure 13 shows the temperature dependences of n_H normalized to the density of charge carriers n field induced in the channel above the threshold and determined from the FET capacitance C_i [Eq. (2)]. The ratio n_H/n is close to unity in the high-temperature (intrinsic) regime [see also Takeya *et al.* (2005)], and decreases with cooling in the trap-dominated regime.

The mobility μ_H determined from Hall-effect measurements is the intrinsic, trap-free mobility μ_0, even if charge transport is significantly affected by trapping. Again, this reflects the fact that the Hall voltage is proportional to the velocity of charge carriers moving between trapping events, and trapped charges do not contribute to the Hall effect. Therefore, in contrast to μ_{eff}, Hall mobility μ_H continues to increase with decreasing T even at low temperatures, where the device enters the trap-dominated regime. In the experiment of Podzorov, Menard, Rogers, and Gershenson (2005), the increase of μ_H with cooling could be traced down to ~150 K; at lower temperatures, Hall measurements were hindered by a rapid increase of $1/f$ fluctuations of the channel conductivity with decreasing temperature in the trap-dominated regime. Observation of a "bandlike" Hall effect suggests that charge transport on the surface of rubrene single crystals occurs via delocalized states over the entire temperature range studied [see, e.g., Pope and Swenberg (1999)].

E. Comparison with the Holstein-Peierls model and transport measurements in the bulk of organic crystals

A microscopic theory of finite-density charge transport on the surface of organic crystals is yet to be developed. However, several models have been proposed for the analysis of low-density (i.e., single-particle) intrinsic transport in the bulk of organic crystals observed in time-of-flight experiments by Karl and co-workers (Karl *et al.*, 1999; Karl, 2001) and, more recently, in the space charge limited current measurements by Jurchescu *et al.* (2004) and de Boer, Jochemsen, *et al.* (2004). Signatures of intrinsic bandlike transport have also been observed in experiments on subpicosecond transient photoconductivity (Thorsmølle *et al.*, 2004; Ostroverkhova *et al.*, 2005). Results of these experiments can be interpreted as an increase of mobility with decreasing temperature (assuming that the efficiency of carrier photogeneration is temperature independent, $\mu \propto T^{-\gamma}$ with $\gamma \sim 0.3$, Ostroverkhova *et al.*, 2005). Note, however, that in the latter experiments, unlike transport measurements, hot (i.e., nonthermalized) optically excited carriers have been probed.

Ab initio calculations of polaron mobility on the basis of the Holstein-Peierls model including a nonlocal electron-lattice coupling (Hannewald and Bobbert, 2004, 2005; see references to earlier work therein) reproduced the temperature-dependent mobility measured in single crystals of naphthalene along different crystalline directions (Karl *et al.*, 1999; Karl, 2001). According to this theory, the mobility for both p- and n-type carriers in polyacenes should exhibit a "metallic" behavior for all T, up to room temperature (with the exception of n-type carriers in naphthalene). Similar behavior was predicted with a semiclassical model developed for the high-temperature regime by Troisi and Orlandi (2006).

Interestingly, the theory of Hannewald and Bobbert also agrees semiquantitatively with the temperature dependence of μ observed in the intrinsic regime for rubrene OFETs. Fitting the Hall mobility data for rubrene OFETs (Fig. 14) with a power-law dependence $\mu(T) \sim T^{-\gamma}$ yields $\gamma \sim 2$ at high temperatures, which agrees with calculations for anthracene and tetracene (Fig. 14). Similar temperature dependences of the hole mobility [$\mu \sim T^{-\gamma}$ with $\gamma \approx (2–2.9)$] were obtained in TOF experiments with bulk ultrapure crystals of naphthalene and perylene by Karl *et al.* (1999) and in recent SCLC mea-

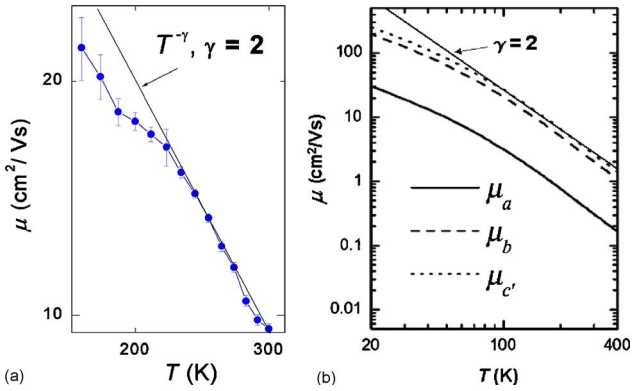

FIG. 14. (Color online) Temperature dependences of the hole mobility in single-crystal organic semiconductors. (a) Hall mobility vs T for a rubrene OFET on a double-logarithm scale (cf. Fig. 13) (Podzorov, Menard, Rogers, and Gershenson, 2005). (b) Calculated T dependences of the mobility for different crystallographic directions in tetracene (Hannewald and Bobbert, 2005).

surements with ultrapure pentacene single crystals by Jurchescu *et al.* (2004) (see Fig. 15).

F. Tuning the intermolecular distance

Realization of the intrinsic conduction regime enables one to study the dependence of polaronic mobility on the intermolecular distance d of the crystal. Note that variations of the polaron mobility with d can only be observed in the intrinsic regime, where trapping is not significant (i.e., $\tau_{tr} \ll \tau$). Recently, continuous "tuning" of the intermolecular distance was achieved in rubrene single-crystal OFETs under applied high pressure P up to 0.5 GPa (Rang *et al.*, 2005); estimates show that at this

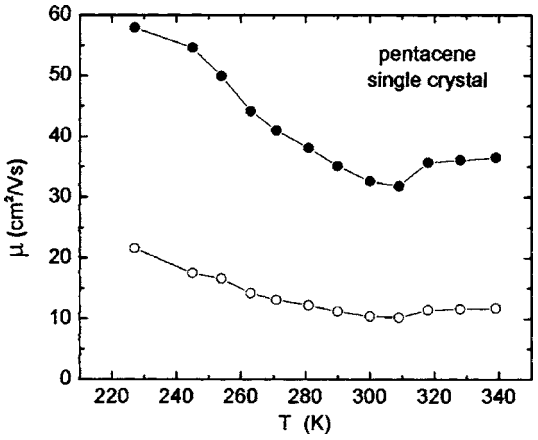

FIG. 15. Temperature dependence of hole mobility in ultrapure pentacene crystals extracted from SCLC measurements (Jurchescu *et al.*, 2004). Open symbols correspond to values of μ calculated for a uniform current distribution across the crystal, solid symbols—assuming a factor of 10^2 anisotropy of conductivity along the ***a*** and ***c*** axes. Below room temperature the mobility increases with decreasing T as $\mu \sim T^{-\gamma}$, where $\gamma \approx 2.4$.

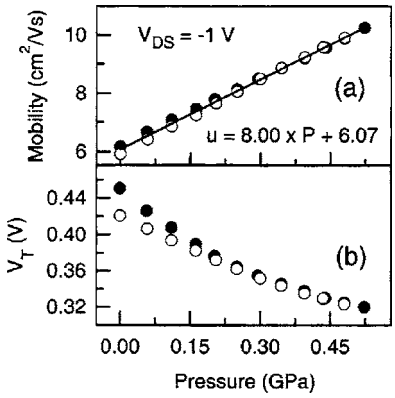

FIG. 16. Pressure dependence of (a) the field-effect mobility, and (b) the threshold voltage in single-crystal rubrene OFETs (solid and open symbols correspond to the increasing and decreasing pressure) (Rang *et al.*, 2005).

pressure the intermolecular distance is decreased by ~1.5%. It has been observed that the mobility increases linearly with P in this pressure range (Fig. 16). This observation is in line with expectations based on polaronic models: The mobility, which is proportional to the square of the transfer integral in the Holstein-type small polaron model, should depend linearly on pressure for small variations in the intermolecular distance d (Rang *et al.*, 2005).

G. Surface versus bulk transport

Semiquantitative agreement between carrier mobilities obtained from OFET measurements and models developed for bulk transport may suggest that there are no differences between polaronic conduction in the bulk and at the surface of organic crystals. However, recent experiments with rubrene single-crystal OFETs (Stassen *et al.*, 2004) revealed a strong dependence of carrier mobility on the dielectric constant ε of the gate insulator. Figure 17 shows that the room-temperature mobility in these devices varies approximately as ε^{-1} over a wide range $\varepsilon = 1-25$. Earlier, a similar trend was observed for organic TFTs based on soluble polymers (Veres *et al.*,

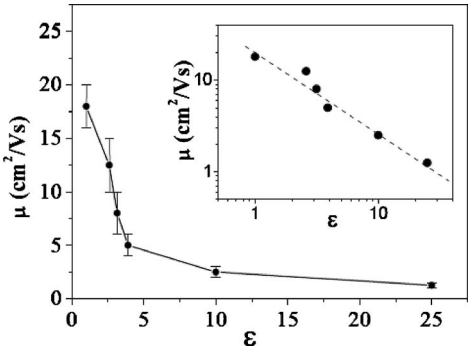

FIG. 17. Dependence of mobility on p-type carriers in rubrene single-crystal OFETs on the dielectric constant of the gate insulator ε (Stassen *et al.*, 2004). Bars represent the spread in mobility values.

2003). [For a recent review of gate dielectrics, including inorganic, polymeric, and self-assembled molecular layers, see Facchetti *et al.* (2005) and Halik *et al.* (2004).] Note that in single-crystal OFETs these observations cannot be attributed to a difference in morphology of the organic semiconductor, since rubrene crystals are always grown under the same conditions, irrespective of the gate insulator used. Thus the observed trend indicates that the mobility of charges at the interface between an organic semiconductor and an insulator is a property of the interface (combination of the semiconductor and insulator) rather than the organic material alone.

It has been predicted that the intrinsic mobility of polarons at the interface with a highly polarizable dielectric may decrease due to an increase of the effective polaronic mass (Houili *et al.*, 2005). Though this prediction is in line with experimental observations, it is worth noting that the effective mobility measured for high-ε OFETs by Stassen *et al.* (2004) and de Boer, Iosad, *et al.* (2005) may be significantly smaller than the intrinsic μ_0 (e.g., because larger densities of shallow traps at organic/dielectric interfaces with greater ε). More experiments in the intrinsic regime are needed to better understand the differences that might exist between transport in the bulk and interface of organic semiconductors.

H. Single-crystal OFETs at high charge-carrier density

Development of single-crystal OFETs enables investigation of several aspects of charge transport in organic semiconductors that could not be addressed in TOF experiments. In particular, OFET-based experiments allow a much broader range of charge-carrier densities to be explored: Approximately one carrier per molecule is technically feasible using high-ε gate dielectrics. At this density, polaron-polaron interactions may play a significant role, which can lead to formation of novel electronic phases. Indeed, it is known that at a sufficiently high density of chemically doped carriers, the potassium-doped fullerene K_xC_{60} exhibits superconductivity ($x=3$) (Hebard *et al.*, 1991) and a Mott-Hubbard insulating state ($x=4$) (Kochanski *et al.*, 1992).

In rubrene single-crystal OFETs, stable operation at a carrier density of $n=5\times10^{13}$ cm^{-2} (corresponding to 0.1 carriers per molecule) has been demonstrated by using a high-quality Ta_2O_5 gate dielectric (Fig. 18) (de Boer, Iosad, *et al.*, 2005). With a breakdown field of $E_{BD}=6.6$ MV/cm and a dielectric constant of $\varepsilon=25$, this material should allow for reaching an even higher density of charge carriers, $\sim10^{14}$ cm^{-2}. However, the presence of moderate leakage currents induces irreversible degradation in the devices currently preventing the operation of Ta_2O_5 gate insulators too close to the breakdown (see Sec. IV.B).

Interestingly, it was observed that in devices with high-ε dielectric the linear increase of the source drain current with the gate voltage saturated at sufficiently high V_G (Fig. 18); for a few devices, I_{SD} even decreased

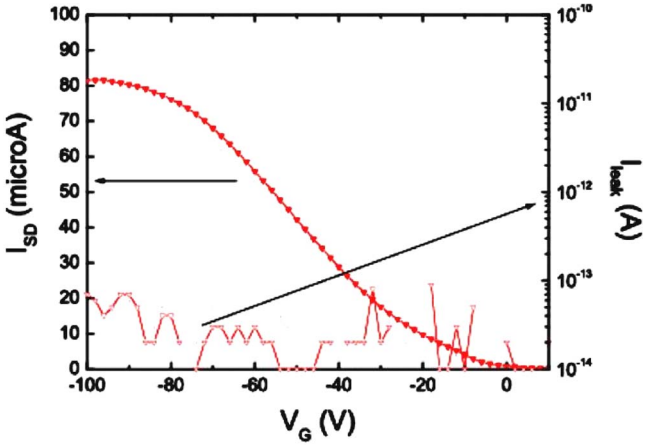

FIG. 18. (Color online) Transfer characteristics $I_{SD}(V_G)$ of a rubrene single-crystal OFET with Ta_2O_5 gate dielectric. At a high density of charge carriers, 5×10^{13} cm^{-2}, a pronounced deviation from the expected linear regime is clearly visible for $V_G<-60$ V. Similar behavior is observed in most devices upon slowly increasing the gate voltage (de Boer, Iosad, *et al.*, 2005).

with increasing V_G. This behavior is reproducible and nonhysteretic, in contrast to the irreversible degradation induced by leakage currents through the gate dielectric described in Sec. IV.B. Even more dramatic nonmonotonic behavior of the channel resistance as a function of the gate voltage has recently been observed for thin-film devices with polymer electrolyte gate dielectric, where the density of field-induced charges may exceed 1×10^{15} cm^{-2} (Panzer and Frisbie, 2005). In particular, the minimum in the channel resistance ($\sim10^7$ $\Omega/\square$) was observed for pentacene-based devices with a hole concentration $\sim1\times10^{15}$ cm^{-2}; the resistance dropped by a factor of 2 with a further increase in the gate voltage. These observations may indicate filling of the conduction band in narrow-band materials at charge concentrations comparable to ~1 charge/molecule, similar to thin-film experiments on chemical doping of organic semiconductors, where the insulator-metal-insulator transition was observed with increasing the concentration of dopants (Craciun, Rogge, den Boer, *et al.*, 2006; Craciun, Rogge, and Morpurgo, 2006).

IV. DEFECTS AT THE SURFACE OF ORGANIC CRYSTALS

Because of the small size of polaronic carriers in molecular crystals, the conduction channel in organic transistors extends in the transverse direction for only one to two molecular layers (Dodabalapur *et al.*, 1995; Dinelli *et al.*, 2004; Kiguchi *et al.*, 2005). For the same reason, polarons interact strongly with chemical impurities and structural defects. As a result, the polaronic transport in organic OFETs is very sensitive to the morphology of semiconductor surface and to the presence of electronic defects at the semiconductor-insulator interface. Carrier trapping, charge doping, molecular reorientation, dipole formation, and a range of possible chemical interactions

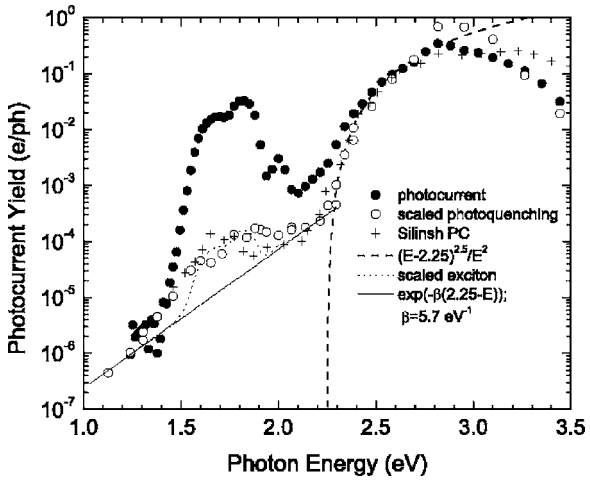

FIG. 19. Energy distribution of localized states in HOMO-LUMO gap of single-crystal pentacene. The HOMO band corresponds to energies >2.25 eV (Lang *et al.*, 2004).

are among the many phenomena that can occur at the semiconductor/insulator interface and affect the electrical characteristics of single-crystal OFETs. For example, localized electronic states within the HOMO-LUMO gap impair the performance of field-effect transistors by increasing the field-effect threshold voltage and reducing the effective mobility of charge carriers [see, e.g., Schmechel and von Seggern (2004)]. The surface density of electronic defects in high-quality single-crystal OFETs can be less than 10^{10} cm^{-2} (Podzorov, Menard, *et al.*, 2004), which corresponds to interdefect distances $\sim$0.1 μm. This low density of surface defects is the major factor that determines the record performance of single-crystal OFET and enables one to explore the fundamental limits of charge carrier transport in organic materials. At the same time, these devices provide an efficient tool to study polaron-defect interactions, as the low density of defects and better control of their nature facilitates interpretation of the experimental data. This section focuses on defects that can be formed in the process of organic crystal growth, OFET fabrication, and as a result of interaction with environmental species.

A. Bulk and surface electronic defects in organic crystals

The density of electronic defects in organic crystals might significantly vary depending on crystal growth methods: Niemax *et al.* (2005) observed using TOF mobility measurements that vapor-grown tetracene single crystals exhibit higher quality than Bridgman-grown crystals. The distribution of localized states in the bulk of organic crystals can be probed by photoconductivity (Silinsh and Čápek, 1994; Pope and Swenberg, 1999; Lang *et al.*, 2004) and space charge limited current (SCLC) measurements (Kao and Hwang, 1981; de Boer, Jochemsen, *et al.*, 2004; Jurchescu *et al.*, 2004). Figure 19 shows photocurrent spectra obtained at room temperature for pentacene crystals in recent experiments by Lang *et al.* (2004). These data indicate a broad ($\sim$1 eV) distribution of localized states within the HOMO-LUMO gap near the HOMO edge, which resembles the exponential "tails" of valence and conduction bands in strongly disordered inorganic semiconductors. This observation raises an issue of environmental stability and degradation of organic semiconductors. A large density of traps in highly purified well-ordered pentacene single crystals might originate from the tendency of pentacene to react with oxygen and water. The sensitivity of pentacene TFTs to gases and vapors has been used in gas sensor applications; it was believed that the diffusion of molecules to the conduction channel along grain boundaries of thin films was necessary for vapor sensing (Crone *et al.*, 2001; Zhu *et al.*, 2002). Recently, however, it was shown using infrared absorption, mass spectrometry, and SCLC measurements that gas molecules from the ambient can even diffuse into single crystals of pentacene over tens of microns, creating doping centers (O_2) or traps (water) (Jurchescu *et al.*, 2005). In particular, it was shown that 6,13-pentacenequinone (the product of pentacene oxidation) forms electronic defects in pentacene, and careful purification of the commercially available material by vacuum sublimation is required to achieve a significant reduction of the 6,13-pentacenequinone impurity (Jurchescu *et al.*, 2004). Following an extensive purification procedure, it has been estimated from SCLC measurements that the bulk density of traps in ultrapure pentacene crystals can be as low as $\sim 2\times 10^{11}$ cm^{-3}. The density of traps can be considerably larger close to the crystal surface, which is normally exposed to air during the OFET assembly process. AFM studies have shown that the surface of pentacene crystals exposed to air for one day is degraded as compared to that of freshly grown (or cleaved) crystals (Jurchescu, 2005).

Interestingly, no surface degradation was observed in AFM experiments with rubrene crystals (Menard *et al.*, 2006), although rubrene also oxidizes in air and forms rubrene endoperoxide in the process of self-sensitized photo-oxidation (Nardello *et al.*, 1999; Podzorov, Pudalov, and Gershenson, 2005). The oxidation of rubrene is restricted to a very thin surface layer (Käffer and Witte, 2005). The role of the surface endoperoxide in charge-transport properties of rubrene OFETs is still unclear. For example, the endoperoxide layer might help to protect the conduction channel from interaction with gas molecules in the environment. Recent experiments with "air-gap" rubrene single-crystal OFETs, in which the conduction channel is fully exposed to environmental species, showed that the channel conductivity is not sensitive to the presence of such gases as O_2, H_2O, N_2, H_2, as well as to saturated vapors of acetone and propanol (Podzorov, Menard, Pereversev, *et al.*, 2005). This remarkable stability of rubrene OFETs is in a sharp contrast with relatively rapid degradation of pentacene devices. The peroxide layer might be also responsible for the formation of a stable built-in conduction channel on free surfaces of rubrene crystals (Podzorov, Pudalov, and Gershenson, 2005).

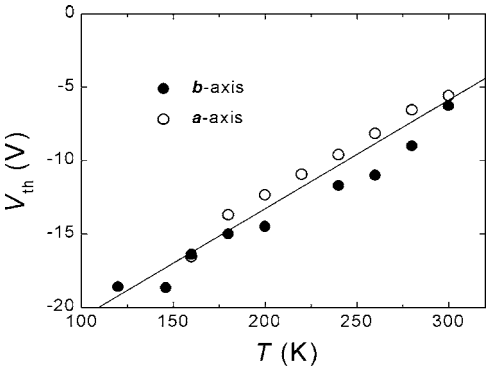

FIG. 20. Temperature dependence of the threshold voltage of a rubrene OFET measured along ***a*** and ***b*** axes in the basal plane of an orthorhombic single crystal (Podzorov, Menard, *et al.*, 2004).

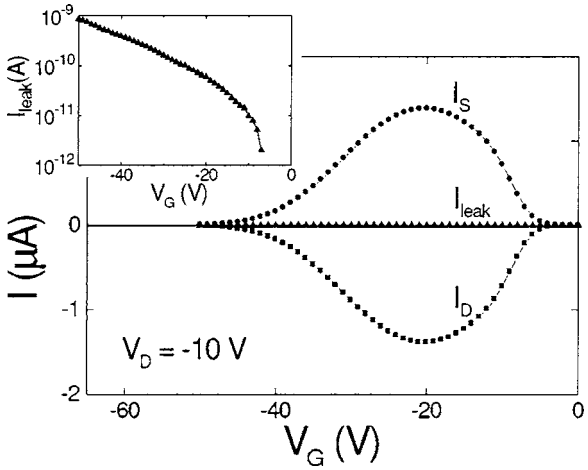

FIG. 21. Source-drain current I_{SD} as a function of V_G in a single-crystal tetracene OFET with Ta_2O_5 gate insulator. Inset: Gate leakage current as a function of V_G. Degradation of the device due to the leakage current results in nonmonotonic transfer characteristics (de Boer, Iosad, *et al.*, 2005).

B. Density of defects in single-crystal OFETs

Photoconductivity and SCLC experiments have been used to obtain information on the localized states in the bulk of organic crystals. However, information on surface states that are relevant to the OFET operation is still very limited. Fortunately, calculation of several basic OFET parameters does not require a detailed knowledge of the trap spectrum. For example, the field-effect threshold voltage is determined by the total density of deep traps N_{tr}^{deep}:

$$V_G^{th} = eN_{tr}^{deep}/C_i. \quad (5)$$

Note that the density of deep traps is a temperature-dependent quantity: The borderline between deep and shallow traps shifts closer to the mobility edge with decreasing T, and any temperature-driven changes of the bandwidth in organic semiconductors would affect the density and spectrum of traps.

The temperature dependence of the threshold voltage of the p-type air-gap rubrene single-crystal OFETs is shown in Fig. 20 (Podzorov, Menard, *et al.*, 2004). At room temperature, the threshold voltage is small; it corresponds to a deep-trap density on the pristine crystal surface $\sim 7\times10^9$ cm^{-2}. The concentration of deep traps increases quasilinearly with cooling up to 2×10^{10} cm^{-2} at 150 K. Assuming that the thickness of the conduction channel does not exceed 1–2 monomolecular layers, the three-dimensional density of traps near the surface at 300 K can be estimated as $\sim 2\times10^{16}$ cm^{-3}.

Defects in molecular materials acting as traps can also be induced during the device operation. Figure 21 shows $I_{SD}(V_G)$ in a tetracene single-crystal transistor with a Ta_2O_5 gate dielectric (de Boer, Iosad, *et al.*, 2005). The source drain current exhibits a nonmonotonic dependence on V_G and is completely suppressed at high values of the gate voltage. Similar behavior has been observed for rubrene and perylene single-crystal devices fabricated using the same gate dielectric. Systematic experiments with differently prepared gate dielectrics have shown that the unusual shape of $I_{SD}(V_G)$ curves was caused by the degradation of the semiconductor surface induced by a leakage current through the gate insulator. Presumably, electrons accelerated in a strong electric field within the gate dielectric gain sufficient kinetic energy to disrupt chemical bonds; these electrons can damage the organic surface and create a large density of deep taps. As the gate voltage is swept to higher values, traps induced by the leakage current cause a substantial increase of the threshold voltage. This damage is irreversible: reducing the gate voltage does not help to restore high channel conductivity.

C. Single-crystal OFETs as a tool to study surface defects

It is well known that x rays create local defects in organic semiconductors by breaking molecules and creating new chemical species. Using this effect, Podzorov, Menard, *et al.* (2004) controllably increased the defect density in the air-gap rubrene single-crystal OFET and studied how this process affected charge transport in these devices (Fig. 22). The x-ray treatment significantly increased the field-effect threshold, and thus the density of deep traps. Interestingly, the charge mobility, which is proportional to the slope of $I_{SD}(V_G)$, and its temperature dependence were not affected by x-ray irradiation. This suggests that deep traps, being filled above the threshold, do not scatter mobile polarons.

Defects in OMCs can be induced not only during crystal growth and handling, but also as a result of processing crystals in a high vacuum environment. In experiments with "vacuum-gap" single-crystal OFETs where the conduction channel was directly exposed to environmental agents, it was observed that both deep and shallow traps could be generated at organic surfaces in vacuum due to interactions with chemically active species produced by high-vacuum gauges or hot surfaces (e.g., resistively heated filaments and evaporation sources) (Podzorov, Menard, Pereversev, *et al.*, 2005).

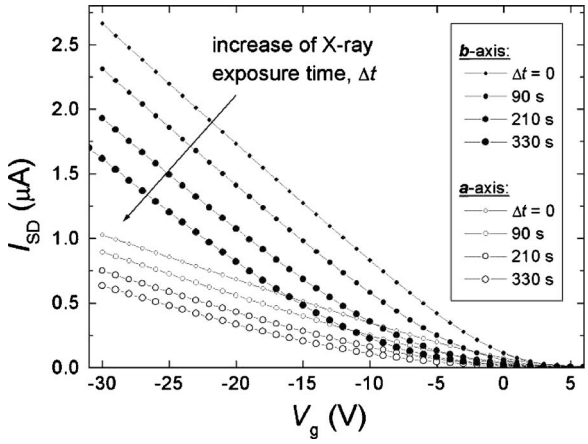

FIG. 22. Effect of a gradual increase of x-ray exposure on the transconductance characteristics of a rubrene OFET. Upon increasing the x-ray dose, the threshold voltage increases, while the mobility remains unchanged (Podzorov, Menard, *et al.*, 2004).

Figure 23 shows that a rapid decrease in the source-drain current of an operating device occurs when a high-vacuum gauge is turned on. The effect has been attributed to interaction of the organic surface with electrically neutral free radicals, produced in the process of hydrocarbon cracking on a hot filament of the gauge with a relatively low activation energy $E_a \sim 2.5$ eV (240 kJ/mol). Clearly, minimization of the damage induced by this defect formation mechanism is important for optimizing the performance for a wide range of thin-film devices of organic and molecular electronic, which are fabricated or characterized in high vacuum.

The experiments described above demonstrate the potential of single-crystal OFETs as a diagnostic tool for studying of phenomena affecting the performance of organic transistors, as well as a tool for studying surface-limited reactions in organic semiconductors.

V. CONCLUSION

Within a short four-year span, the development of single-crystal organic field-effect transistors significantly

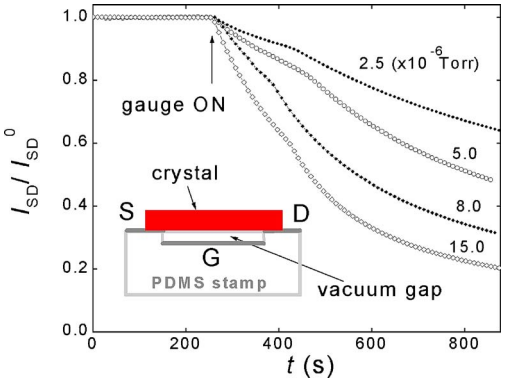

FIG. 23. (Color online) Gauge effect: Time evolution of I_{SD} of an operating organic field-effect transistor with exposed channel, recorded at different pressures P in the chamber. The hot-cathode high vacuum gauge was turned on at $t=250$ s (Podzorov, Menard, Pereversev, *et al.*, 2005).

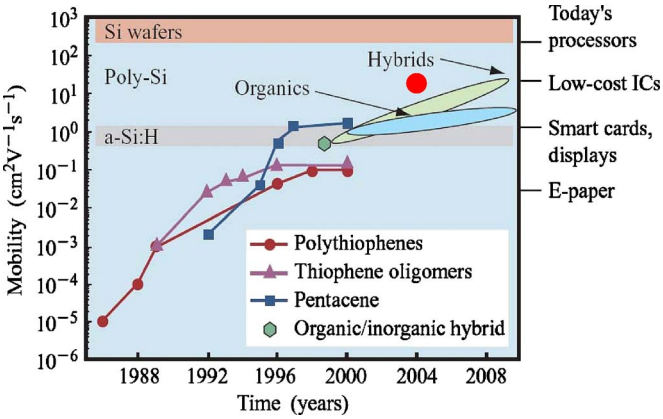

FIG. 24. (Color online) Realization of charge transport not limited by static defects is crucial for better understanding of the fundamental limits of organic electronics. The (red) dot on the figure borrowed from the IBM Journal for Research and Development, January 2001 (Shaw and Seidler, 2001), represents the room-temperature mobility in rubrene single-crystal OFETs, the only intrinsic mobility found in the field-effect experiments up to date.

advanced our understanding of transport processes on organic surfaces and shed light on fundamental limits of organic devices (Fig. 24). Due to their reproducibility, single-crystal OFETs enabled the systematic study of polaronic effects in a broad range of parameters, bridging the gap between the fundamental research on ultrapure bulk crystals and applied research on thin-film transistors. The potential applications of single-crystal OFETs go far beyond the fundamental research on polaronic transport. These devices are very useful for studying surface-limited reactions and defect formation on organic surfaces (Podzorov, Menard, Pereversev, *et al.*, 2005), light-induced effects in organic semiconductors (Podzorov and Gershenson, 2005; Podzorov, Pudalov, and Gershenson, 2005), and work-function engineering on organic surfaces (Takeya *et al.*, 2004).

Although the single polaron problem was one of the early subjects of interest for condensed-matter physics 50 years ago, the physics of polaronic gases and liquids at a finite density remains a complex and poorly understood topic even these days, with many open questions. The research on organic single-crystal OFETs addresses these questions in a class of materials that are currently of great technological relevance. Below we briefly mention some specific issues that are now starting to be within experimental reach due to the development of single-crystal OFETs and for which theoretical work remains to be done.

One important issue is studying the electronic density of states. Many examples of band-structure calculations can be found in the literature for different molecular crystals. However, these calculations do not include the interaction between the electronic and vibrational degrees of freedom, so that it remains to be understood how polaronic effects affect the density of states and the width of HOMO and LUMO bands. These quantities are expected to exhibit nontrivial temperature depen-

dences due to the strongly T-dependent parameters of polarons in Holstein-like models.

Another important issue is the transport across metal/organic interfaces (Cahen *et al.*, 2005). For inorganic semiconductors, our understanding of contacts with metals is based on the concept of Schottky barrier. For organic semiconductors based on small molecules, the experimental data remain, to a large extent, unclear and irreproducible because of the poor interface control. Because of the narrow bandwidth in organic semiconductors and weak van der Waals coupling between molecule and metal, the behavior of metal/organic interfaces is likely to be qualitatively different from their inorganic counterparts. Owing to their high reproducibility, single-crystal OFETs have great potential to clarify the situation in this field. Note that these questions are directly related to the issue of contact resistance in organic transistors that imposes serious limitations on the downscaling of organic thin-film devices (Bürgi *et al.*, 2003).

The development of single-crystal OFETs capable of operating at liquid-He temperatures remains an experimental challenge. In experiments performed so far, the statistics of a polaronic gas was Boltzmann-like due to the combination of a large density of states in narrow bands, relatively low density of carriers, and high temperatures. The development of more advanced techniques for the purification of molecular materials will enable the expansion of the intrinsic transport regime to much lower temperature, where effects of quantum statistics and polaron-polaron interactions should become experimentally accessible.

The development of high-quality single-crystal OFETs will be crucial for comparative studies of different molecular materials and, in particular, for testing transport properties of newly synthesized molecular materials. This testing is essential for supporting the effort on synthesizing more soluble small organic molecules that are attractive for applications, such as soluble derivatives of linear acenes (Klare *et al.*, 2003; Moon *et al.*, 2004; Payne *et al.*, 2005). Systematic efforts in this direction will require the investigation of a much broader variety of new molecular compounds. Single-crystal OFETs provide a unique tool for the express analysis of transport characteristics of new molecular materials (similar experiments with thin-film devices would require time-consuming and expensive work on improving the film morphology). Therefore even though fabrication of devices compatible with large scale manufacturing is based on thin films, the research on single-crystal OFETs can play an important role in the material selection for applications. The case of rubrene perfectly illustrates this point. The unprecedented quality of OFETs based on vapor-grown rubrene single crystals has stimulated work on the deposition of rubrene thin films from solution: recently, mobility $\sim 0.7\ \mathrm{cm}^2/\mathrm{V\,s}$ at room temperature was demonstrated for solution-processed rubrene thin-film transistors (Stingelin-Stutzmann *et al.*, 2005).

Many important fundamental and applied issues have been left outside the scope of this Colloquium. One of these issues is the interaction of organic transistors with light. Despite the fact that organic transistors are intended to operate primarily in optoelectronic devices (e.g., active-matrix displays), surprisingly little is known about light-induced effects in OFETs. In thin-film organic transistors, light illumination produced a weak photoconductivity response [see, e.g., Narayan and Kumar (2001)], reduces the threshold voltage (Hamilton and Kanicki, 2004; Saragi *et al.*, 2004; Noh *et al.*, 2005), and reverses the (dark) bias stress effect (Salleo and Street, 2003; Street *et al.*, 2003). Large concentration of defects in organic films that trap light-generated carriers and/or act as recombination centers complicate these experiments and their interpretation. Single-crystal OFETs with a low density of traps have a potential to become an indispensable tool for studying fundamental photoinduced processes at organic surfaces and interfaces. Work in this direction has been already initiated: Two light-induced effects were recently observed in single-crystal OFETs (Podzorov and Gershenson, 2005; Podzorov, Pudalov, and Gershenson, 2005).

ACKNOWLEDGMENTS

We are indebted to our collaborators for their significant contributions to the work reported here, especially to R. W. I. de Boer, N. Iosad, T. M. Klapwijk, E. Menard, V. M. Pudalov, J. A. Rogers, and A. F. Stassen. M.E.G. and V.P. at Rutgers University were supported in part by NSF Grant No. DMR-0405208 and Grant No. ECS-0437932; A.F.M. acknowledges financial support from FOM and from NWO via the Vernieuwingsimpuls 2000 program.

REFERENCES

Agranovich, V. M., and G. F. Bassani, 2003, *Electronic Excitations in Organic Based Nanostructures* (Elsevier Academic, New York).

Aleshin, A. N., J. Y. Lee, S. W. Chu, J. S. Kim, and Y. W. Park, 2004, Appl. Phys. Lett. **84**, 5383.

Bao, Z., A. J. Lovinger, and A. Dodabalapur, 1996, Appl. Phys. Lett. **69**, 3066.

Brédas, J. L., J. P. Calbert, D. A. da Silva Filho, and J. Cornil, 2002, Proc. Natl. Acad. Sci. U.S.A. **99**, 5804.

Bube, R. H., 1960, *Photoconductivity in Solids* (Wiley, New York).

Bürgi, L., T. J. Richards, R. H. Friend, and H. Sirringhaus, 2003, J. Appl. Phys. **94**, 6129.

Butko, V. V., X. Chi, D. V. Lang, and A. P. Ramirez, 2003, Appl. Phys. Lett. **83**, 4773.

Cahen, D., A. Kahn, and E. Umbach, 2005, Mater. Today **8** (7,8), 32.

Campbell, R. B., J. Monteath Robertson, and J. Trotter, 1962, Acta Crystallogr. **15**, 289.

Chapman, B. D., A. Checco, R. Pindak, T. Siegrist, and C. Kloc, 2006, J. Cryst. Growth **290**, 479.

Cheng, Y. C., R. J. Silbey, D. A. da Silva Filho, J. P. Calbert, J. Cornil, and J. L. Brédas, 2003, J. Chem. Phys. **118**, 3764.

Chesterfield, R. J., C. R. Newman, T. M. Pappenfus, P. C. Ewbank, M. H. Haukaas, K. R. Mann, L. L. Miller, and C. D. Frisbie, 2003, Adv. Mater. (Weinheim, Ger.) **15**, 1278.

Chua, L. L., J. Zaumseil, J. F. Chang, E. C.-W. Ou, P. K.-H. Ho, H. Sirringhaus, and R. Friend, 2005, Nature (London) **434**, 194.
Craciun, M. F., S. Rogge, M.-J. L. den Boer, S. Margadonna, K. Prassides, Y. Iwasa, and A. F. Morpurgo, 2006, Adv. Mater. (Weinheim, Ger.) **18**, 320.
Craciun M. F., S. Rogge, and A. F. Morpurgo, 2006, e-print cond-mat/0603261.
Crone, B., A. Dodabalapur, A. Gelperin, L. Torsi, H. E. Katz, A. J. Lovinger, and Z. Bao, 2001, Appl. Phys. Lett. **78**, 2229.
da Silva Filho, D. A., E.-G. Kim, and J.-L. Bredas, 2005, Adv. Mater. (Weinheim, Ger.) **17**, 1072.
de Boer, R. W. I., M. E. Gershenson, A. F. Morpurgo, and V. Podzorov, 2004, Phys. Status Solidi B **201**, 1302.
de Boer, R. W. I., N. N. Iosad, A. F. Stassen, T. M. Klapwijk, and A. F. Morpurgo, 2005, Appl. Phys. Lett. **86**, 032103.
de Boer, R. W. I., M. Jochemsen, T. M. Klapwijk, A. F. Morpurgo, J. Niemax, A. K. Tripathi, and J. Pflaum, 2004, J. Appl. Phys. **95**, 1196.
de Boer, R. W. I., T. M. Klapwijk, and A. F. Morpurgo, 2003, Appl. Phys. Lett. **83**, 4345.
de Boer, R. W. I., A. F. Stassen, M. F. Craciun, C. L. Mulder, A. Molinari, S. Rogge, and A. F. Morpurgo, 2005, Appl. Phys. Lett. **86**, 262109.
Deng, W.-Q., and W. A. Goddard, 2004, J. Phys. Chem. B **108**, 8614.
de Wijs, G. A., C. C. Mattheus, R. A. de Groot, and T. T. M. Palstra, 2003, Synth. Met. **139**, 109.
Dinelli, F., M. Murgia, P. Levy, M. Cavallini, and F. Biscarini, 2004, Phys. Rev. Lett. **92**, 116802.
Dodabalapur, A., L. Torsi, and H. E. Katz, 1995, Science **268**, 270.
Emin, D., 1982, Phys. Today **35** (6), 34.
Facchetti, A., M.-H. Yoon, and T. J. Marks, 2005, Adv. Mater. (Weinheim, Ger.) **17**, 1705.
Forrest, S. R., 2004, Nature (London) **428**, 911.
Fratini, S., and S. Ciuchi, 2003, Phys. Rev. Lett. **91**, 256403.
Goldmann, C., S. Haas, C. Krellner, K. P. Pernstich, D. J. Gundlach, and B. Batlogg, 2004, J. Appl. Phys. **96**, 2080.
Halik, M., H. Klauk, U. Zschieschang, G. Schmid, C. Dehm, M. Schuetz, S. Maisch, F. Effenberger, M. Brunnbauer, and F. Stellacci, 2004, Nature (London) **431**, 963.
Hamilton, M. C., and J. Kanicki, 2004, IEEE J. Sel. Top. Quantum Electron. **10**, 840.
Hannewald, K., and P. A. Bobbert, 2004, Appl. Phys. Lett. **85**, 1535.
Hannewald, K., and P. A. Bobbert, 2005, in *Physics of Semiconductors*, edited by J. Menendez and C. G. van de Walle, AIP Conf. Proc. No. 772 (AIP, Melville, NY), p. 1101.
Hebard, A. F., M. J. Rosseinsky, R. C. Haddon, D. W. Murphy, S. H. Glarum, T. T. M. Palstra, A. P. Ramirez, and A. R. Kortan, 1991, Nature (London) **350**, 600.
Henn, D. E., W. G. Williams, and D. J. Gibbons, 1971, J. Appl. Crystallogr. **4**, 256.
Holstein, T., 1959, Ann. Phys. (N.Y.) **8**, 343.
Hoppe, H., and N. S. Sariciftci, 2004, J. Mater. Res. **19**, 1924.
Horowitz, G., 2004, J. Mater. Res. **19**, 1946.
Horowitz, G., M. E. Hajlaoui, and R. Hajlaoui, 2000, J. Appl. Phys. **87**, 4456.
Houili, H., J. D. Picon, M. N. Bussac, and L. Zuppiroli, 2005, e-print cond-mat/0510751.
Jurchescu, O. D., 2005, private communication.
Jurchescu, O. D., J. Baas, and T. T. M. Palstra, 2004, Appl. Phys. Lett. **84**, 3061.
Jurchescu, O. D., J. Baas, and T. T. M. Palstra, 2005, Appl. Phys. Lett. **87**, 052102.
Kao, K. C., and W. Hwang, 1981, *Electrical Transport in Solids* (Pergamon, New York), Vol. 14.
Käffer, D., and G. Witte, 2005, Phys. Chem. Chem. Phys. **7**, 2850.
Karl, N., 2001, in *Organic Electronic Materials*, edited by R. Farchioni and G. Grosso (Springer-Verlag, Berlin), pp. 283–326.
Karl, N., K.-H. Kraft, J. Marktanner, M. Much, F. Schatz, R. Stehle, and H. M. Uhde, 1999, J. Vac. Sci. Technol. A **17**, 2318.
Katz, H. E., 2004, Chem. Mater. **16**, 4748.
Kenkre, V. M., J. D., Andersen, D. H. Dunlap, and C. B. Duke, 1989, Phys. Rev. Lett. **62**, 1165.
Kiguchi, M., M. Nakayama, T. Shimada, and K. Saiki, 2005, Phys. Rev. B **71**, 035332.
Klare, J., G. Tulevski, A. de Picciotto, K. White, and C. Nuckolls, 2003, J. Am. Chem. Soc. **125**, 6030.
Kochanski, G. P., A. F. Hebard, R. C. Haddon, and A. T. Fiory, 1992, Science **255**, 184.
Lang, D. V., X. Chi, T. Siegrist, A. M. Sergent, and A. P. Ramirez, 2004, Phys. Rev. Lett. **93**, 086802.
Laudise, R. A., Ch. Kloc, P. G. Simpkins, and T. Siegrist, 1998, J. Cryst. Growth **187**, 449.
Mas-Torrent, M., P. Hadley, S. T. Bromley, X. Ribas, J. Tarres, M. Mas, E. Molins, J. Veciana, and C. Rovira, 2004, J. Am. Chem. Soc. **126**, 8546.
Meijer, E. J., D. M. De Leeuw, S. Setayesh, E. van Veenendaal, B.-H. Huisman, P. W. M. Blom, J. C. Hummelen, U. Scherf, and T. M. Klapwijk, 2003, Nat. Mater. **2**, 678.
Menard, E., A. Marchenko, V. Podzorov, M. E. Gershenson, D. Fichou, and J. A. Rogers, 2006, Adv. Mater. (Weinheim, Ger.) **18**, 1552.
Menard, E., V. Podzorov, S.-H. Hur, A. Gaur, M. E. Gershenson, and J. A. Rogers, 2004, Adv. Mater. (Weinheim, Ger.) **16**, 2097.
Misewich, J. A., R. Martel, Ph. Avouris, J. C. Tsang, S. Heinze, and J. Tersoff, 2003, Science **300**, 783.
Moon, H., R. Zeis, E.-J. Borkent, C. Besnard, A. J. Lovinger, T. Siegrist, Ch. Kloc, and Z. Bao, 2004, J. Am. Chem. Soc. **126**, 15322.
Nakamura, K., M. Ichikawa, R. Fushiki, T. Kamikawa, M. Inoue, T. Koyama, and Y. Taniguchi, 2005, Jpn. J. Appl. Phys., Part 2 **44**, L1367.
Narayan, K. S., and N. Kumar, 2001, Appl. Phys. Lett. **79**, 1891.
Nardello, V., M. J. Marti, C. Pierlot, and J. M. Aubry, 1999, J. Chem. Educ. **76**, 1285.
Nelson, S. F., Y.-Y. Lin, D. J. Gundlach, and T. N. Jackson, 1998, Appl. Phys. Lett. **72**, 1854.
Neuman C. R., C. D. Frisbie, D. A. Da Silva Filho, J.-L. Bredas, P. C. Ewbank, and K. R. Mann, 2004, Chem. Mater. **16**, 4436.
Niemax, J., A. K. Tripathi, and J. Pflaum, 2005, Appl. Phys. Lett. **86**, 122105.
Noh, Y.-Y., D.-Y. Kim, Y. Yoshida, K. Yase, B.-J. Jung, E. Lim, and H.-K. Shim, 2005, Appl. Phys. Lett. **86**, 043501.
Ostroverkhova, O., D. G. Cooke, S. Shcherbyna, R. F. Egerton, F. A. Hegmann, R. R. Tykwinski, and J. E. Anthony, 2005, Phys. Rev. B **71**, 035204.
Payne, M. M., S. R. Parkin, J. E. Anthony, C. C. Kuo, and T.

N. Jackson, 2005, J. Am. Chem. Soc. **127**, 4986 (2005).
Panzer M. J., and C. D. Frisbie, 2005, J. Am. Chem. Soc. **127**, 6960.
Podzorov, V., and M. E. Gershenson, 2005, Phys. Rev. Lett. **95**, 016602.
Podzorov, V., M. E. Gershenson, Ch. Kloc, R. Zeis, and E. Bucher, 2004, Appl. Phys. Lett. **84**, 3301.
Podzorov, V., E. Menard, A. Borissov, V. Kiryukhin, J. A. Rogers, and M. E. Gershenson, 2004, Phys. Rev. Lett. **93**, 086602.
Podzorov, V., E. Menard, S. Pereversev, B. Yakshinsky, T. Madey, J. A. Rogers, and M. E. Gershenson, 2005, Appl. Phys. Lett. **87**, 093505.
Podzorov, V., E. Menard, J. A. Rogers, and M. E. Gershenson, 2005, Phys. Rev. Lett. **95**, 226601.
Podzorov, V., V. M. Pudalov, and M. E. Gershenson, 2003, Appl. Phys. Lett. **82**, 1739.
Podzorov, V., V. M. Pudalov, and M. E. Gershenson, 2005, Appl. Phys. Lett. **85**, 6039.
Podzorov, V., S. E. Sysoev, E. Loginova, V. M. Pudalov, and M. E. Gershenson, 2003, Appl. Phys. Lett. **83**, 3504.
Pope, M., and C. E. Swenberg, 1999, *Electronic Processes in Organic Crystals and Polymers*, 2nd ed. (Oxford University Press, New York).
Rang, Z., M. I. Nathan, P. P. Ruden, V. Podzorov, M. E. Gershenson, C. R. Newman, and C. D. Frisbie, 2005, Appl. Phys. Lett. **86**, 123501.
Riordan, M., and L. Hoddeson, 1997, *Crystal Fire: The Birth of Information Age* (Norton, New York).
Salleo, A., and R. A. Street, 2003, J. Appl. Phys. **94**, 471.
Saragi, T. P. I., R. Pudzich, T. Fuhrmann, and J. Salbeck, 2004, Appl. Phys. Lett. **84**, 2334.
Schmechel, R., and H. von Seggern, 2004, Phys. Status Solidi B **201**, 1215.
Shaw, J. M., and P. F. Seidler, 2001, IBM J. Res. Dev. **45**, 3.
Sheats, J. R., 2004, J. Mater. Res. **19**, 1974.
Shur, M., M. Hack, and J. G. Shaw, 1989, J. Appl. Phys. **66**, 3371.
Silinsh, E. A., and V. Čápek, 1994, *Organic Molecular Crystals: Interaction, Localization, and Transport Phenomena* (AIP, New York).
Stassen, A. F., R. W. I. de Boer, N. N. Iosad, and A. F. Morpurgo, 2004, Appl. Phys. Lett. **85**, 3899.
Stingelin-Stutzmann, N., E. Smith, H. Wondergem, C. Tanase, P. Blom, P. Smith, and D. de Leeuw, 2005, Nat. Mater. **4**, 601.
Street, R. A., A. Salleo, and M. L. Chabinyc, 2003, Phys. Rev. B **68**, 085316.
Sundar, V. C., J. Zaumseil, V. Podzorov, E. Menard, R. L. Willett, T. Someya, M. E. Gershenson, and J. A. Rogers, 2004, Science **303**, 1644.
Sze, S. M., 1981, *Physics of Semiconductor Devices* (Wiley, New York).
Takahashi, T., T. Takenobu, J. Takeya, and Y. Iwasa, 2006, Appl. Phys. Lett. **88**, 033505.
Takeya, J., C. Goldmann, S. Haas, K. P. Pernstich, B. Ketterer, and B. Batlogg, 2003, J. Appl. Phys. **94**, 5800.
Takeya, J., K. Tsukagoshi, Y. Aoyagi, T. Takenobu, and Y. Iwasa, 2005, Jpn. J. Appl. Phys., Part 2 **44**, L1393.
Takeya, J., T. Nishikawa, T. Takenobu, S. Kobayashi, Y. Iwasa, T. Mitani, C. Goldmann, C. Krellner, and B. Batlogg, 2004, Appl. Phys. Lett. **85**, 5078.
Thorsmølle, V. K., R. D. Averitt, X. Chi, D. J. Hilton, D. L. Smith, A. P. Ramirez, and A. J. Taylor, 2004, Appl. Phys. Lett. **84**, 891.
Troisi, A., and G. Orlandi, 2006, Phys. Rev. Lett. **96**, 086601.
Troisi, A., G. Orlandi, and J. E. Anthony, 2005, Chem. Mater. **17**, 5024.
Veres, J., S. D. Ogier, S. W. Leeming, D. C. Cupertino, and S. M. Khaffaf, 2003, Adv. Funct. Mater. **13**, 199.
Wehrli, S. and C. Helm, 2004, J. Appl. Phys. **95**, 5621.
Wu, M. W., and E. M. Conwell, 1997, Chem. Phys. Lett. **266**, 363.
Yasuda, T., and T. Tsutsui, 2005, Chem. Phys. Lett. **402**, 395.
Zeis, R., C. Besnard, T. Seigrist, C. Schlockermann, X. Chi, and Ch. Kloc, 2006, Chem. Mater. **18**, 244.
Zeis, R., T. Siegrist, and Ch. Kloc, 2005, Appl. Phys. Lett. **86**, 022103.
Zhu, Z.-T., J. T. Mason, R. Dieckmann, and G. G. Malliaras, 2002, Appl. Phys. Lett. **81**, 4643.